arXiv:astro-ph/9810394v1 23 Oct 1998

Submitted to the *P. A. S. P.*

Combining Undersampled Dithered Images

Tod R. Lauer
National Optical Astronomy Observatories[1], P. O. Box 26732, Tucson, AZ 85726
Electronic mail: lauer@noao.edu

ABSTRACT

Undersampled images, such as those produced by the *HST* WFPC-2, misrepresent fine-scale structure intrinsic to the astronomical sources being imaged. Analyzing such images is difficult on scales close to their resolution limits and may produce erroneous results. A set of "dithered" images of an astronomical source generally contains more information about its structure than any single undersampled image, however, and may permit reconstruction of a "superimage" with Nyquist sampling. I present a tutorial on a method of image reconstruction that builds a superimage from a complex linear combination of the Fourier transforms of a set of undersampled dithered images. This method works by algebraically eliminating the high order satellites in the periodic transforms of the aliased images. The reconstructed image is an exact representation of the data-set with no loss of resolution at the Nyquist scale. The algorithm is directly derived from the theoretical properties of aliased images and involves no arbitrary parameters, requiring only that the dithers are purely translational and constant in pixel-space over the domain of the object of interest. I show examples of its application to WFC and PC images. I argue for its use when the best recovery of point sources or morphological information at the *HST* diffraction limit is of interest.

Subject headings: image processing

1. Introduction

It's nice to work with well-sampled astronomical images. A well-sampled image can be readily resampled to various scales, orientations, or more complex geometries without loss of information. Its spatial resolution is well-understood, permitting a clear analysis of the relative contributions of information and noise. Further, many image processing algorithms will only work on well-sampled

[1]The National Optical Astronomy Observatories are operated by the Association of Universities for Research in Astronomy, Inc., under cooperative agreement with the National Science Foundation.

data. In some cases, however, it's not practical or even desirable to obtain well-sampled images. Given detectors with a finite number of pixels and significant readout noise, one may prefer to trade-off resolution for increased field size or photometric sensitivity. Both considerations were central to the design of the *HST* WFPC-1 and WFPC-2 cameras, to give examples of instruments that produce undersampled astronomical images. WFPC-2 in particular has generated the largest library of high-resolution optical astronomical images to date, but ironically the severe undersampling in the WFC system, and the still less than critical sampling of the PC at all but the reddest wavelengths, limit the resolution of *HST* observations as much as the telescope optics, themselves.

There is no magic that can undo the undersampling in a single image; analysis of such data always requires respect for their peculiarities. At the same time, it may be possible to obtain additional observations with the same camera system that contain information lost in the original images. For example, if the camera can be offset by a fraction of a pixel over a sequence of exposures or "dithered," one can observe how the structure of objects in the image varies with respect to their positions on the pixel-grid, and thus recover details not contained in any single image. This suggests that one might construct a well-sampled super-image from a set of undersampled, but dithered images.

In general, when the size of a pixel is important with respect to the intrinsic point-spread function (PSF), the image as observed is

$$I(x, y) = O(x, y) * P(x, y) * \Pi(x, y), \tag{1}$$

where O is the intrinsic projected appearance of the astronomical field being imaged, P is the PSF due to the telescope and camera optics, and Π is the spatial form of the pixel itself, (which is often assumed to be a uniform square, although this need not be the case), and $*$ means convolution. Both P and Π limit the resolution of I and thus implicitly specify the minimum sampling requirements — a dilemma if Π is too big, since it sets what the sampling really is, regardless of what's needed. If the astronomical scene and camera are time-stable, however, dithering the camera allows proper sampling of the field *convolved with the pixel response* as well as the PSF, to be obtained. If the camera is pointed on a fine and regular $n \times n$ grid of sub-pixel steps, where n is the number of substeps within the original large pixel, then the images can be simply interleaved into a super-image that has small pixels equal to the dither step-size. If the step-size is small enough, the super-image will be critically sampled. A simple way to view this is to consider an image consisting of the astronomical field just convolved with the PSF due to the optics alone. The sampling would be done on pixels equal to the size of the dither step, chosen to be fine enough to ensure critical sampling. The image is then blurred by the original pixel response. Drawing every n^{th} pixel in x and y clearly recreates one of the dithered images as actually created by the camera. Therefore, conversely interleaving the dithered images creates the well-sampled super-image.

In practice, however, it may not be possible to step the camera in a regular pattern. Sub-pixel

dithers have been used in many WFPC-2 programs, for example, but were often not executed with enough precision to fall on a regular pattern; simple interlacing of the image-set cannot be done in such cases. This problem is critical for the *Hubble Deep Field* (HDF) observations (Williams et al. 1996). A regular dither was specified, but did not actually occur.

To solve the problem of combining images with an irregular dither pattern, a *Drizzle*-algorithm was developed (Williams et al. 1996; Fruchter & Hook 1998) that works by simply dropping or "drizzling" the pixels in any single image onto a finer grid, offsetting the image by the actual sub-pixel step obtained, slicing up its pixels as they fall on the finer grid. The *Drizzle* algorithm worked well, producing the now famous well-sampled full-color image of the HDF. The *Drizzle* algorithm is appealing, as it is intuitive — one is just shifting and overlapping the images on a fine grid, shrinking the original pixels small enough so as to minimize any blurring associated with forcing the pixels into the new grid, but keeping them big enough so that there are no "holes" of empty data in the new super image. Further, because *Drizzle* works in the spatial domain, it's easy to correct for cosmic ray events, hot pixels, or any other data missing in any single images, as well as correcting for any geometric distortion. Development of *Drizzle* represents a significant improvement in the software available to astronomers for analyzing undersampled images, and has greatly improved the recovery of information from *HST* images.

Despite the success of *Drizzle,* however, it is frankly justified on intuitive rather than formal theoretical grounds, and indeed depends on two *ad hoc* parameters, namely the spacing of the super-image grid and the size of the pixels to be drizzled. It also introduces its own blurring function, Π', which *statistically* is about the size of the super-image pixel; in detail, the actual resolution for any object depends on how it falls with respect to the final grid. Although Π' in practice may be much smaller than Π, it still may be large compared to the PSF and introduce significant blurring in its own right. These issues were indeed discussed in the context of the HDF, and limit its deconvolution or interpretation of its power spectrum on the finest scales.

In attempt to develop an algorithm that both mines better resolution from the data, and stands on a solid theoretical foundation, I present a method that reconstructs a super-image from an arbitrary set of dithered observations with no-degradation of resolution. This method is only a modest extension to two-dimensional data of a method for recovering one-dimensional functions from undersampled data presented by Bracewell (1978). The method works by computing the Fourier transform of the super-image as a linear combination of the transforms of the individual images; the aliased components are eliminated algebraically. I have also extended the method to estimate the super-image when it is actually overdetermined by the dithered observations. None of this is particularly complex, and not surprizingly, the professional image processing literature already contains discussions of this method (see Tsai & Huang 1984, or Kim et al. 1990). However, given the strong interest in using dithers in the context of *HST* imaging, I considered it worthwhile to present this paper as a tutorial on the method of Fourier algebraic reconstruction and explore its use in the context of *HST* observations.

2. The Theory of Reconstructing an Image From Aliased Data-sets

2.1. The Sampling of a 1-D Function

To understand how to reconstruct an image from undersampled data, I start by considering the effects of sampling on a 1-D function, $f(x)$. For reconstruction to work, $f(x)$ must be band-limited, so that its Fourier transform,

$$\overline{f(x)} = F(u) = \int_{-\infty}^{\infty} f(x) e^{-2\pi i x u} dx, \tag{2}$$

is non-zero only for $-u_c < u < u_c$, where u_c is the critical frequency. If x is expressed in terms of pixels, then sampling at every integer pixel is sufficient provided that $u_c < 1/2$. This can be understood by considering the Fourier transform of the sampled function, The sampling of $f(x)$ is equivalent to multiplying it by a *shah*-function,

$$\mathrm{III(ax)} \equiv \frac{1}{|\mathrm{a}|} \sum_{\mathrm{n}=-\infty}^{+\infty} \delta\left(\mathrm{x} - \frac{\mathrm{n}}{\mathrm{a}}\right), \tag{3}$$

where $a = 1$ for the specific case of integer-pixel sampling. The Fourier transform of the sampled function is then,

$$\begin{aligned} \overline{f(x) \cdot \mathrm{III(x)}} &= F(u) * \mathrm{III(u)}, \\ &= \sum_{n=-\infty}^{+\infty} F(u-n), \end{aligned} \tag{4}$$

where I have used the fact that the transform of a shah-function is itself a shah-function. As is well-known, the Fourier transform of a sampled function is periodic, repeating over the entire frequency domain. If $f(x)$ is band-limited, however, none of the copies or satellites of $F(u)$ overlap. The satellites are spaced at each integer-step in u, but the requirement that $u_c < 1/2$, means that they also reach zero before crossing over the midpoint of the interval (Figure 1). This condition is no longer obeyed when the sampling interval is larger than each integer pixel step. For example, if every other pixel is sampled, then,

$$\begin{aligned} \overline{f(x) \cdot \mathrm{III}\left(\frac{\mathrm{x}}{2}\right)} &= F(u) * \mathrm{III(2u)}, \\ &= 2 \sum_{n=-\infty}^{+\infty} F\left(u - \frac{n}{2}\right). \end{aligned} \tag{5}$$

The transformed shah-function now samples at every half-integer step in the Fourier domain, causing strong overlaps or *aliasing* between the satellites of $F(u)$ (Figure 1). If $f(x)$ is unknown, the full extent of its transform cannot be deduced from the aliased sample, which in turn means that the sample is itself an incomplete representation of $f(x)$.

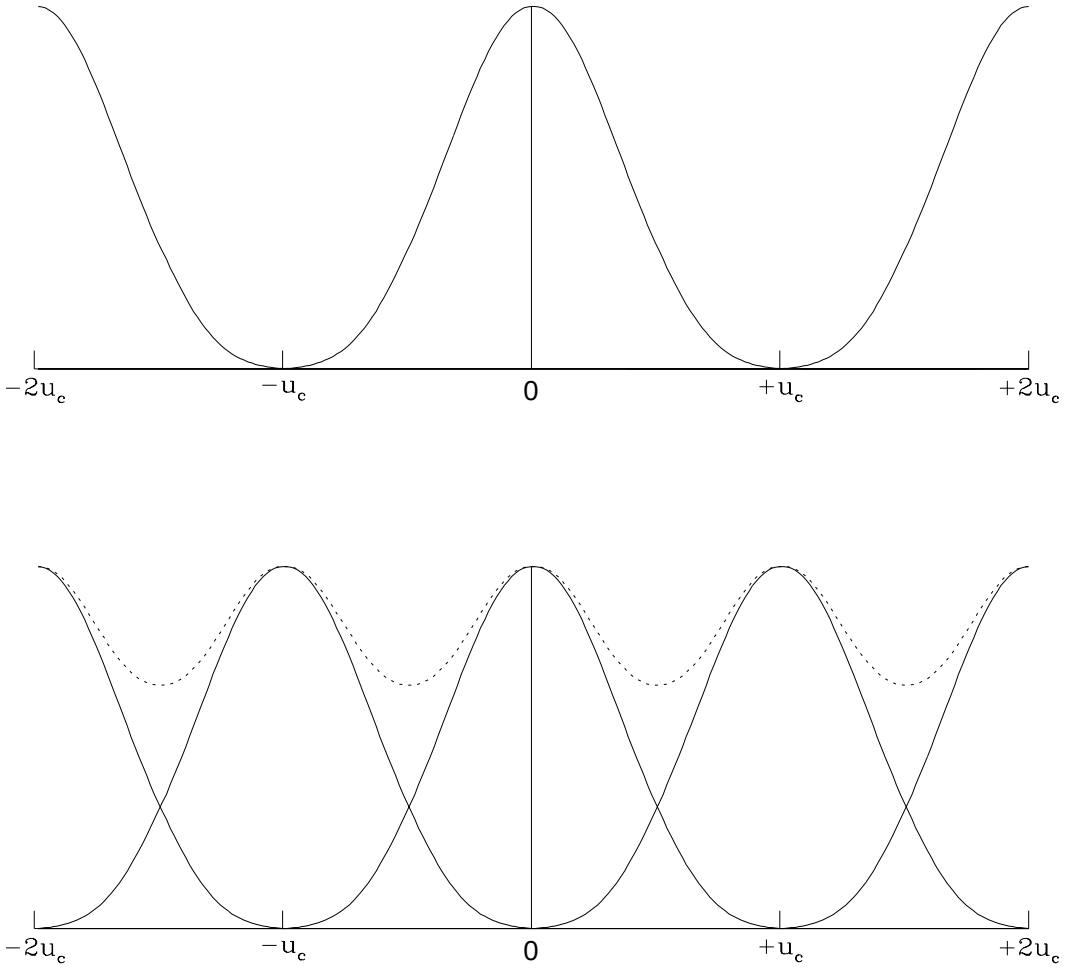

Fig. 1.— This figure schematically shows the effects of sampling on the Fourier power spectrum of a continuous 1-D function. Sampling causes the power spectrum to be periodic, with the period inversely proportional to the spatial sampling frequency. When the function is well-sampled, the satellites occur at intervals of $2u_c$, or greater, where u_c is the critical frequency, or the highest frequency at which the intrinsic function has non-zero power (upper graph). With coarser sampling, the function becomes undersampled and the satellites begin to overlap. With $2\times$ undersampling (bottom graph) the satellites occur at every integer multiple of u_c. The total transform (dotted) is the sum over all satellites and is severely aliased.

2.2. Recovery of a 1-D Function

Bracewell (1978) shows that a function can be recovered from collection of undersampled data-sets given prior knowledge of u_c (as might exist given a detector pixel shape and optical point-spread function), provided that the sampling among the various data-sets is interlaced by some fraction of the sampling interval and that the basic sampling interval is not too sparse compared to u_c. Consider again the alternate pixel sample above (which I relabel as $d_0(x)$). For the fundamental interval $-1/2 < u < 1/2$,

$$\begin{aligned} D_0(u) &= \overline{f(x) \cdot \mathrm{III}\left(\frac{\mathrm{x}}{2}\right)}, \\ &= \frac{1}{2}\left(F(u-\frac{1}{2}) + F(u) + F(u+\frac{1}{2})\right). \end{aligned} \tag{6}$$

Since I have specified that $F(u)$ is band-limited to $|u| < 1/2$, for $0 \le u < 1/2$,

$$D_0(u) = \frac{1}{2}\left(F(u-\frac{1}{2}) + F(u)\right), \tag{7}$$

and for $-1/2 < u < 0$,

$$D_0(u) = \frac{1}{2}\left(F(u) + F(u+\frac{1}{2})\right). \tag{8}$$

Now let there be a second data set that also samples $f(x)$ with alternate pixel spacing, but spatially offset from the $d_0(x)$ samples by some $x_0 \neq 2n$ (one might presume $0 < x_0 < 2$, but this is not required). The transform of the new data-set, $d_{x_0}(x)$, is

$$\begin{aligned} D_{x_0}(u) &= \overline{f(x) \cdot \mathrm{III}\left(\frac{\mathrm{x}}{2} - \mathrm{x}_0\right)}, \\ &= F(u) * \overline{\left(\mathrm{III}\left(\frac{\mathrm{x}}{2}\right) * \delta(\mathrm{x} - \mathrm{x}_0)\right)}, \\ &= F(u) * \left(\mathrm{III}\,(2\mathrm{u}) \cdot \mathrm{e}^{-2\pi \mathrm{i u x}_0}\right). \end{aligned} \tag{9}$$

This reduces to

$$D_{x_0}(u) = \frac{1}{2}\left(F(u) + e^{-\pi i x_0} F(u-\frac{1}{2})\right), \qquad 0 \le u < 1/2, \tag{10}$$

$$= \frac{1}{2}\left(F(u) + e^{+\pi i x_0} F(u+\frac{1}{2})\right), \qquad -1/2 < u < 0. \tag{11}$$

Note that $d_{x_0}(x)$ is no less aliased than is $d_0(x)$, but since the overlap portion has a differing phase, the transforms of the two samples can be combined to solve for the transform of $f(x)$,

$$F(u) = 2\,\frac{D_{x_0}(u) - e^{-\pi i x_0} D_0(u)}{1 - e^{-\pi i x_0}}, \qquad 0 \le u < 1/2, \tag{12}$$

$$= 2\,\frac{D_{x_0}(u) - e^{+\pi i x_0} D_0(u)}{1 - e^{+\pi i x_0}}, \qquad -1/2 < u < 0. \tag{13}$$

In other words, one can reconstruct $f(x)$ exactly from two data-sets offset from each other, each undersampled by a factor two. Note that in the special case, where $x_0 = 1$, $d_0(x)$ holds the even-numbered pixels and $d_{x_0}(x)$ holds the odd-numbered ones, then

$$F(u) = D_{x_0}(u) + D_0(u), \tag{14}$$

as would be expected, since the sum in equation (4) can clearly be separated this way. With exact interlacing, one can just add the transforms of the two individual data-sets (provided that the transform preserves their relative phases).

2.3. Recovery of an Image

This method can be directly generalized to the case of reconstructing a 2-D image. The shah-function becomes a 2-D regular grid of δ-functions, and the two-dimensional Fourier transform of an image is:

$$\overline{f(x,y)} = F(u,v) = \int_{-\infty}^{\infty}\int_{-\infty}^{\infty} f(x,y)e^{-(2\pi ixu+2\pi iyv)}dx\ dy. \tag{15}$$

If there is an observation $d_{x_1,y_1}(x,y)$ that is factor of two undersampled in both x and y (thus having 1/4 of the pixels of the critically sampled image), and offset by $x_1,\ y_1$ from the nominal grid defining $f(x,y)$, then in the domain $0 \le u < 1/2,\ 0 \le v < 1/2$,

$$\begin{aligned} D_{x_1,y_1}(u,v) &= \frac{1}{4}\Big(F(u,v) + e^{-\pi ix_1}F(u-\frac{1}{2},v) \\ &\quad + e^{-\pi iy_1}F(u,v-\frac{1}{2}) + e^{-\pi i(x_1+y_1)}F(u-\frac{1}{2},v-\frac{1}{2})\Big). \end{aligned} \tag{16}$$

There are analogous expressions in the other three quadrants of the u,v plane; however, for real-valued images, half of the u,v plane will simply be the complex conjugate of the other half and thus need not be computed (see Figure 2). As can be seen, with four data-sets, each having a unique offset in x *or* y, it is again possible to eliminate the overlap contributions. This requires solving a system of equations with complex coefficients:

$$\frac{1}{4}\begin{pmatrix} 1 & e^{-\pi ix_1} & e^{-\pi iy_1} & e^{-\pi i(x_1+y_1)} \\ 1 & e^{-\pi ix_2} & e^{-\pi iy_2} & e^{-\pi i(x_2+y_2)} \\ 1 & e^{-\pi ix_3} & e^{-\pi iy_3} & e^{-\pi i(x_3+y_3)} \\ 1 & e^{-\pi ix_4} & e^{-\pi iy_4} & e^{-\pi i(x_4+y_4)} \end{pmatrix}\mathbf{F} = \mathbf{D}, \tag{17}$$

where $\mathbf{F}$ is a 4-vector holding $F(u,v)$ in the first position, followed by the u, v, and lastly u,v satellites, $\mathbf{D}$ is a 4-vector of the transforms of the 4 undersampled data-sets. One can then invert this matrix to find

$$F(u,v) = \sum_{n=1}^{4} c_n D_{x_n,y_n}(u,v), \tag{18}$$

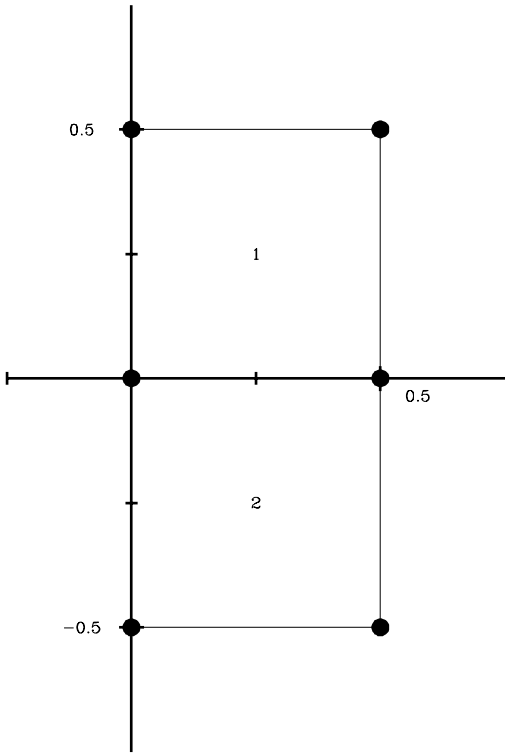

Fig. 2.— This figure schematically shows the configuration of the Fourier domain for reconstructing an image with 2×2 subsampling. For real images, Fourier transforms need only be calculated for the semi-plane with $0 \leq u \leq 1/2$, $-1/2 < v \leq 1/2$ (this presumes that the x-axis transform is computed first), where the frequencies are defined with respect to the pixels of the reconstructed image. Each image in the observed set is aliased, and has satellites at all integer multiples of $(u, v) = 1/2$ in the Fourier domain, with each satellite having significant power over $\Delta u = \pm 1/2$, and $\Delta v = \pm 1/2$ about its central location. The figure shows as heavy dots the central location of all satellites that overlap with the fundamental transform centered at $(u, v) = 0$. Algebraic elimination of the satellites is done in two regions, marked 1 and 2; the satellites that contribute to a given region are those at its corners.

where c_n will be a complex coefficient. Solution for the second quadrant is analogous — the phases differ only in sign, being positive when the domain of the frequency is negative. As an example, for the special case of where the four data-sets contain the exact interlaces of integer pixels in x and y, $\mathbf{F}$ and $\mathbf{D}$ are more simply related as:

$$\frac{1}{4}\begin{pmatrix} 1 & 1 & 1 & 1 \\ 1 & -1 & 1 & -1 \\ 1 & 1 & -1 & -1 \\ 1 & -1 & -1 & 1 \end{pmatrix} \mathbf{F} = \mathbf{D}, \tag{19}$$

which has the solution, as expected of

$$F(u,v) = \sum_{n=1}^{4} D_{x_n,y_n}(u,v). \tag{20}$$

2.4. Recovery of an Image Overdetermined by the Data

Four images determine $F(u,v)$, exactly, but if one actually has additional images available, $F(u,v)$ is overdetermined, and a least squares solution is required. This means finding the $F(u,v)$ that minimizes the norm

$$E = \|\mathbf{\Phi F} - \mathbf{D}\,\|, \tag{21}$$

where, as above $\mathbf{\Phi}$ is the matrix of phases. In this case, however, $\mathbf{\Phi}$ is now an $n \times 4$ matrix,

$$\mathbf{\Phi} = \frac{1}{4}\begin{pmatrix} 1 & e^{-\pi i x_1} & e^{-\pi i y_1} & e^{-\pi i (x_1+y_1)} \\ 1 & e^{-\pi i x_2} & e^{-\pi i y_2} & e^{-\pi i (x_2+y_2)} \\ \vdots & \vdots & \vdots & \vdots \\ 1 & e^{-\pi i x_n} & e^{-\pi i y_n} & e^{-\pi i (x_n+y_n)} \end{pmatrix}, \tag{22}$$

where $n \geq 4$ is the number of data-sets, and $\mathbf{D}$ is now a vector of length n holding the data-sets; $\mathbf{F}$ is still the same 4-vector. Expanding equation (21) gives

$$\begin{aligned} E^2 &= (\mathbf{\Phi F} - \mathbf{D}\,)^H (\mathbf{\Phi F} - \mathbf{D}\,) \\ &= \mathbf{F}^H \mathbf{\Phi}^H \mathbf{\Phi F} - \mathbf{F}^H \mathbf{\Phi}^H \mathbf{D} - \mathbf{D}^H \mathbf{\Phi F} + \mathbf{D}^H \mathbf{D}, \end{aligned} \tag{23}$$

where H denotes the Hermitian (or complex-conjugate) transpose. Minimizing E implies

$$\mathbf{F} = \left(\mathbf{\Phi}^H \mathbf{\Phi}\right)^{-1} \mathbf{\Phi}^H \mathbf{D}. \tag{24}$$

In the case of an overdetermined situation, one might further want to weight the observations differently. For example, it may not be practical to obtain exposures of identical length over the sequence of observations, or they may have variable backgrounds. In this case, it's easy to generalize equation (24) to include weighting, giving

$$\mathbf{F} = \left(\mathbf{\Phi}^H \mathbf{W}^T \mathbf{W} \mathbf{\Phi}\right)^{-1} \mathbf{\Phi}^H \mathbf{W}^T \mathbf{W} \mathbf{D}, \tag{25}$$

where $\mathbf{W}$ is an $n \times n$ matrix of weights and $\mathbf{W}^T$ is its transpose (the weights are real-valued). $\mathbf{W}$ can account for any covarience between the images, but it is most likely to be diagonal on the presumption that the individual images will probably be independent.

2.5. Generalization to Higher Degress of Subsampling

Double sampling is likely to be sufficient to remove modest aliasing, but higher levels of subsampling may be required when the undersampling is severe. Generalization to finer levels of subsampling is straight forward, if somewhat tedious. As the observed images become coarser with respect to the reconstructed image, the aliased satellites become closer together and overlap more severely. Algebraic elimination of the satellites requires identifying all satellites contributing power to a given location in the Fourier domain. In practice, this means slicing the Fourier domain into an increasingly large number of subsets. Figure 3 sketches out the structure of the Fourier domain for 3×3 subsampling. In the 3×3 case, the Fourier domain is divided into six regions, with nine differing satellites contributing to $\mathbf{F}$ in each one; at least $n \geq 9$ dithered images will be required to find a solution, and $\mathbf{\Phi}$ is will now be an $n \times 9$ matrix. An important distinction between the 2×2 and 3×3 cases, is that in the former, since the satellites are spaced exactly by u_c, only the six satellites that are visible within the Fourier semi-domain need be considered. In the 3×3 case, the satellites are separated only by multiples of $2u_c/3$, thus the first set of satellites with their *centers* actually falling outside the semi-domain will still overlap with it.

3. Implementation of the Fourier Image Reconstruction

3.1. Data-set Requirements

The present reconstruction method works only if the data satisfies a number of conditions, the most important of which is that the intrinsic image structure remain constant over the extent of the dithered data-taking sequence. The PSF should not vary significantly in time, or if the dither steps are large, in space as well. "Significantly" in this context means variations on spatial scales where the Fourier S/N ratio is greater than unity; bright point sources are more vulnerable to PSF-variations than faint or more diffuse sources. Bright noise spikes, hot pixels, cosmic ray hits, or any other variable sources, must also be eliminated or repaired prior to reconstruction. A final obvious requirement is that reconstruction can work only on the portions of the dither set in common to all images; as the dither takes place, it is likely that a larger region of the sky will be imaged than is present on any single image — subimages of the common overlap region must be isolated prior to reconstruction.

The mathematics of the Fourier reconstruction method do not strictly require that the angular size of the pixels be constant over the extent of any image, provided that the dither steps

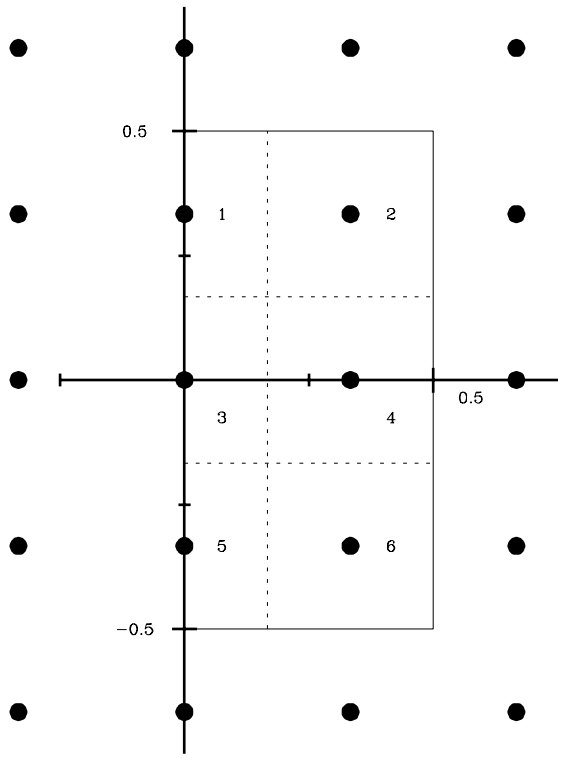

Fig. 3.— As for the 2×2 case, this figure schematically shows the configuration of the Fourier domain for reconstructing an image with 3×3 subsampling. Again, the Fourier transforms are calculated only for the semi-plane with $0 \leq u \leq 1/2$, $-1/2 < v \leq 1/2$. Satellites now occur at all integer multiples of $(u, v) = 1/3$, but each satellite still has significant power over $\Delta u = \pm 1/2$, and $\Delta v = \pm 1/2$ about its central location. The figure shows as heavy dots the central location of all satellites that overlap with the fundamental transform centered at $(u, v) = 0$. Algebraic elimination of the satellites is now done in six regions; the satellites that contribute to a given region are the one at its center, and the eight surrounding it.

are small enough that they can be regarded as constant over the complete area of the images. Images that have variations in their pixel scale large enough so that the amplitude of the dithers (in pixels) varies significantly over the extent of the image must be processed in subsets small enough that the dithers can be regarded as constant over the angular domain selected. Lastly, the dithers must be translational only, with no rotation.

The reader familiar with *Drizzle* may object that these requirements are too restrictive for many sets of dithered data. *Drizzle* performs cosmic ray event and defect rejection, as well as geometric rectification, when building a sub-sampled image. *Drizzle* is thus attractive for the complete reduction of panoramic data sets. This issue will be discussed further in §4, but I emphasize that the present approach is solely concerned with the specific task of accurate reconstruction of a Nyquist-sampled image. Geometric rectification or defect rejection are problems that can be separated from the actual reconstruction algorithm; the caveats presented above do not necessarily prevent use of the present method if they can be addressed apart from the reconstruction task.

Two other requirements on the data set concern the pattern and measurement of the dithers. Ideally, the fractional portion of the dither steps (that is ignoring the integer number of pixels stepped over) should match the nominal 2×2 or 3×3 equal sub-stepping patterns as closely as possible; or if the problem is heavily overdetermined be at least evenly spread over the area of a single pixel. In this case, solution of equation (25) will generate a set of complex coefficients, c_n of nearly equal power (presuming equal weights). Formally solutions can be calculated for any nondegenerate dither pattern; however, as the dither pattern moves away from optimal, the images will be combined unevenly, with heavy weight being placed on those with less redundant positions. For real images, this means that the relative noise contributed by such images will be amplified compared to others in the dither set. Noise properties of the reconstructed image will be discussed below; in practice, excess amplification of noise is only important for large departures from an ideal pattern.

Accurate measurement of the dither steps is required to construct the Φ matrix. This may be done iteratively. Initially one might use simple centroids of stars or other compact objects within a given image to measure dither offsets. Once a reconstructed image has been generated, it can be cross-correlated with the individual images to refine the offsets; permitting a more accurate reconstruction to be done in a second iteration.

3.2. Computing the Reconstructed Image

Given the prepared set of dithered images and measured dither steps, computation of the reconstructed image can proceed. In practice I have done this within the Vista image processing system, making use of its native image arithmetic and Fourier routines, augmenting it only with a new subroutine to construct Φ, and then solve for and apply c_n to the Fourier transform of a given

image.

For each image, the first steps are to normalize it to a common exposure level, and to then expand it into a sparse array, spacing out the pixels by 2× or 3× as desired. Each pixel in an input image then occupies one of the corners of a cell of 2×2 or 3×3 new pixels in the expanded image, with the other $n \times n - 1$ pixels in each cell set to zero. This actualizes each image as a sparse III function; one can see that for exact $n \times n$ dithers, the other images would simply be interlaced at the vacant locations.

Once an image is expanded, its Fourier transform is computed; a power spectrum at this stage clearly shows the aliased satellites. The next step is to multiply the transform by c_n, remembering that different coefficients must be used for the various regions within the domain. The adjusted transform is then added to the adjusted transforms of the other images. The reconstructed image is the inverse transform of the complete sum.

One important caveat is that each the transform of each image must be multiplied by a complex phase, $\exp\left(-2\pi K i \left(x_j + y_j\right)\right)$, where (x_j, y_j) is its spatial offset from the average of the other images, and K is the degree of subsampling. This is required because the mathematics presented in the previous section presume a two-dimensional coordinate system anchored to the sky, rather than the grid of the detector. In other words, as each image is expanded, initially its III function has identical coordinates to those in the other images, with the object apparently moving with respect to the detector coordinate system. This step resets the coordinate system to that of the sky, correctly phasing the various III functions of the dither set.

3.3. Examples of Reconstructed Images

Figures 4 and 5 show PC and WFC PSFs reconstructed from a calibration program of 20 F555W dithered images of a field within the ω Cen globular cluster. The PC PSF was reconstructed with 2×2 subsampling, while 3×3 subsampling was used for the WFC PSF. The cores of the PSFs are now well resolved, and no "boxy" artifacts are seen as can occur in *Drizzle* reconstructions (Fruchter & Hook 1998). It's also worthwhile to note the strong blurring introduced by the WFC pixel function, Π, itself. Again, the reconstruction does not recover the intrinsic PSF due to the optics only, but the intrinsic PSF convolved with Π. The PC PSF clearly has the sharper and rounder core, while the center of the WFC PSF is strongly determined by the pixel shape.

Figure 6 shows the power spectra at various stages in the reconstruction of the WFC PSF to illustrate the algorithm concretely. The final combination of 20 images has reduced the contribution of the aliased satellites by $\sim 10^5$. The final power spectrum also ratifies the strong contribution of the WFC pixel to the total PSF. The shape of the spectrum is clearly boxy; further, the central lobe is surrounded by a strong zero, which would be expected in the power spectrum of a nearly square and uniform pixel function.

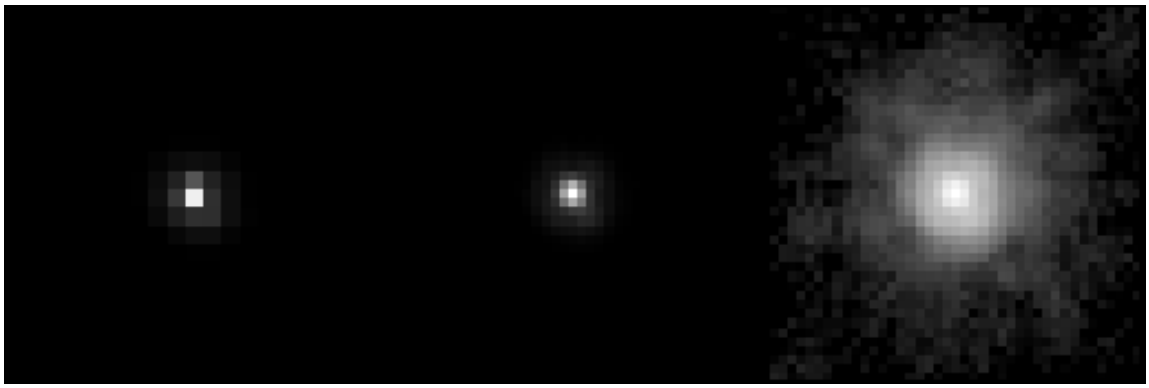

Fig. 4.— Reconstruction of the *HST* PC PSF with 2×2 subsampling is shown based on 20 dithered F555W images of a star in ω Cen. The image at left shows a linear stretch of one of the PSF images (selected to be nearly centered on a pixel). The central image shows the reconstructed PSF with the same intensity stretch. The last image is a logarithmic stretch (with dynamic range 3.5 in log units) of the reconstructed PSF.

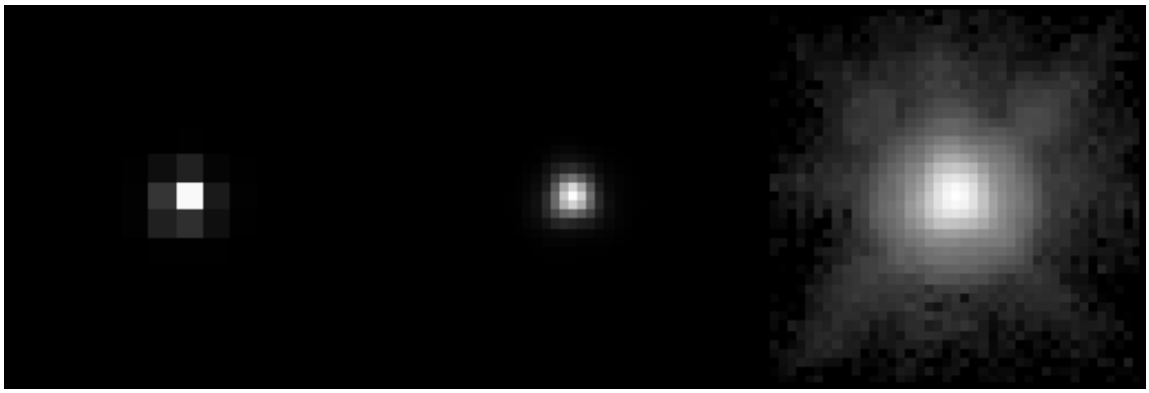

Fig. 5.— Reconstruction of the *HST* WFC PSF with 3×3 subsampling is shown based on 20 dithered F555W images of a star in ω Cen. The image at left shows a linear stretch of one of the PSF images (selected to be nearly centered on a pixel). The central image shows the reconstructed PSF with the same intensity stretch. The last image is a logarithmic stretch (with dynamic range 3.5 in log units) of the reconstructed PSF.

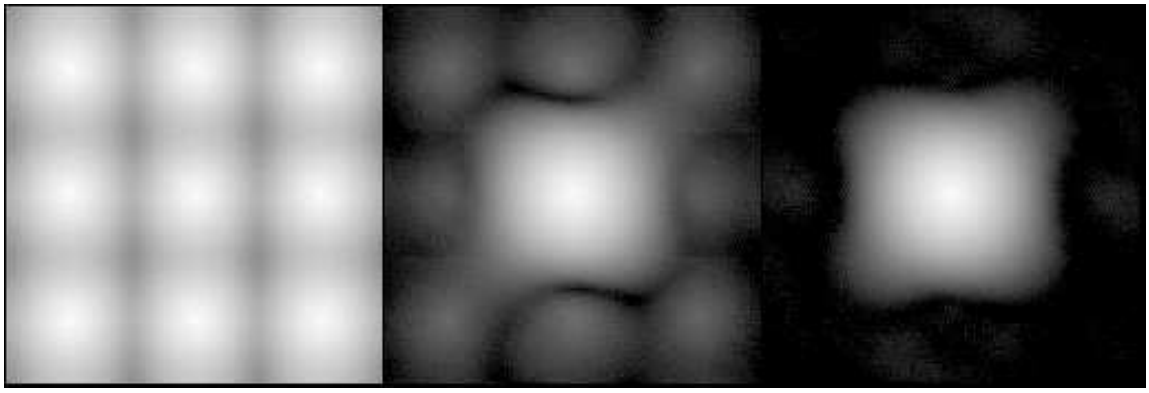

Fig. 6.— Power spectra are shown at various stages in the reconstruction of the WFC PSF with 3×3 subsampling. The left image shows the power spectrum of a single PSF image expanded as a sparse III function. The low contrast of the minima between the bright peaks of the satellites shows the effects of the severe aliasing in WFC images. The middle image shows the spectrum of the penultimate reconstruction. At this stage 19 of the 20 images have been combined and the flanking satellites have been greatly reduced in power. The right image shows the power spectrum of the final reconstructed PSF — the partial combination shown in the middles has now been completed by the addition of the last image. The display scale is identical and logarithmic (with a range of 10^5) for all three spectra. The power spectra are shown for the full Fourier domain for ease of visual interpretation, even though the transforms are computed only in a semi-plane.

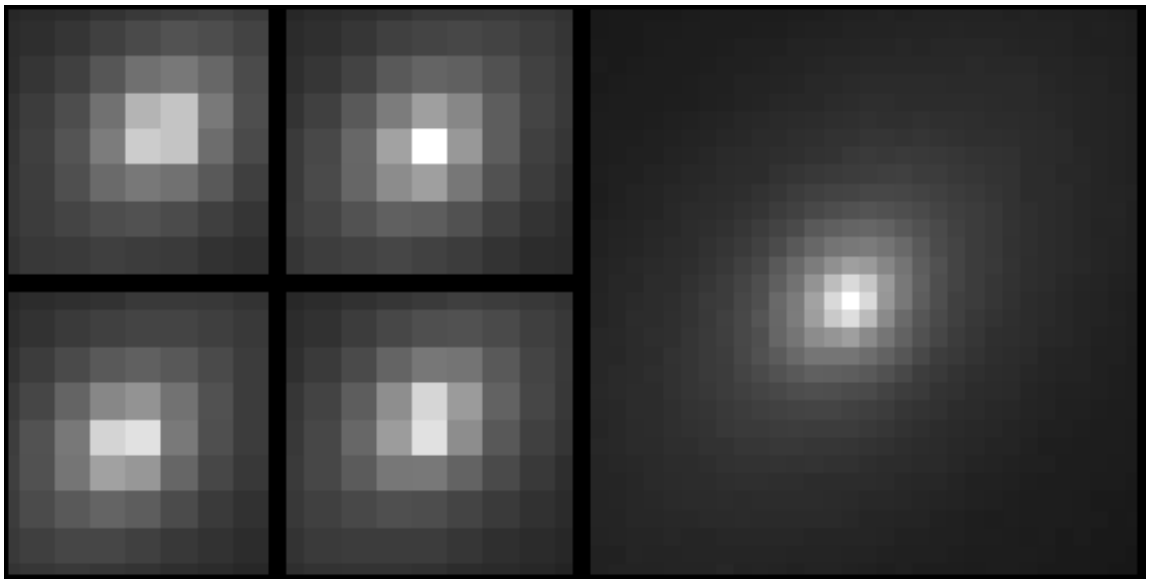

Fig. 7.— The reconstruction of the center of NGC 1023 with 2×2 subsampling. Five F555W PC images were used. Four of the images (shown at left) define an approximate 2×2 interlace pattern; however, the offsets typically differed from the nominal 0.5 pixel steps by ~ 0.1 pixel (the fifth image falls within 0.1 pixel of one of the four images shown). The stretch is linear.

Turning to more interesting objects, Figure 7 shows the 2×2 reconstruction of the nucleus of the early-type galaxy NGC 1023. Unlike the situation for the PSFs, which were highly overdetermined, only five dithered images were available for NGC 1023. The dither pattern was close to a nominal exact interlace, but the offsets typically differed from the nominal 0.5 pixel by ~ 0.1 pixel, thus the present method was required. This galaxy has a particularly compact center (Lauer et al. 1995). The present observations were obtained to observe its central structure with the best resolution available — reconstructing the image without introducing additional blurring is thus critical. The reconstructed image clearly shows the sharp compact nucleus of NGC 1023, but is also smooth and free from artifact; indeed this image can now be processed further with PSF deconvolution.

Lastly, I show a 2×2 reconstruction of a chain-galaxy at $z = 1.355$ (Cohen et al. 1996) in the *Hubble Deep Field* (Figure 8), along with a *Drizzle* reconstruction. [2] Superficially the two images look identical; the gross morphology is not strongly dependent on the reconstruction algorithm. Detailed comparison shows, however, that the present reconstruction is slightly sharper

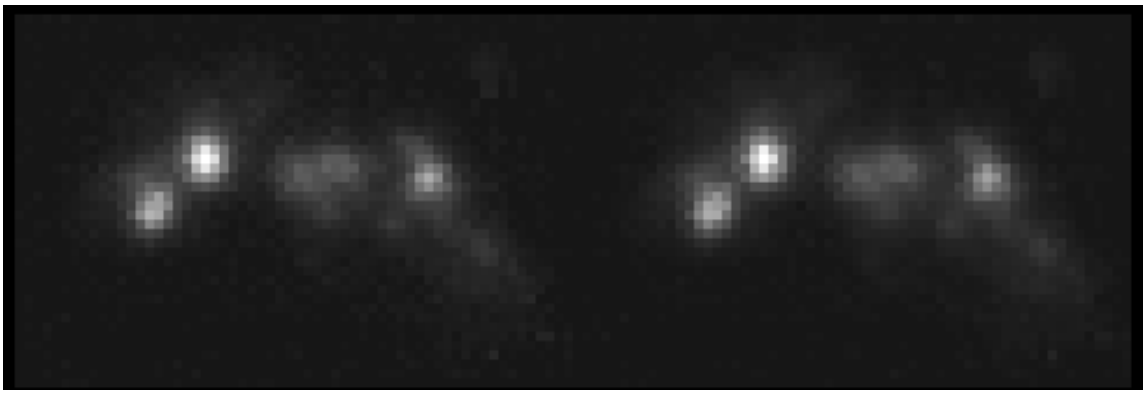

Fig. 8.— Two reconstructions of a $z = 1.355$ chain galaxy in the *Hubble Deep Field* with 2×2 subsampling, based on 11 F450W WFC images. The left image was done with the present Fourier method, while the image on the right is a *Drizzle* reconstruction. The stretch is linear.

— the peak of the brightest knot in the image is $\sim 7\%$ brighter, for example. Matching the resolution of the *drizzled* image requires smoothing the Fourier reconstruction with a Gaussian with $FWHM \approx 1$ pixel (on the subsampled scale). The Fourier reconstruction does appear to have more noise, but again this is due to the smoothing inherent in the *Drizzle* algorithm. The Fourier reconstruction can be smoothed, but one of the nice things about having a well-sampled image is that optimal filters can be used to improve its appearance. A Weiner filter, for example, can be used to reject much of the noise in the present image with little effect on its resolution; an

[2]The *Drizzle* reconstruction shown was done with the same image set, weights, and pixel grid used for the Fourier reconstruction, and differs from the *Drizzle*-reconstructed image of the same galaxy in the official release of the *HDF.*

option that is not possible with aliased images.

A more general comparison of the present method to *Drizzle* is complex, as the difference between the two depends on the dither pattern, the size of the image set, choice of the reconstructed pixel size, and the *Drizzle* drop size. For example, when the dither pattern is close to an exact interlace, *Drizzle* can be configured to produce a simple interlaced reconstruction, while at the opposite end of the scale, *Drizzle* can do simple "shift-and-add" reconstructions on the original pixel scale, which implies highly significant smoothing. In general, it appears from a number of additional experiments that when a large image set is available, *Drizzle* effectively smooths a perfect reconstruction with a gaussian with width of about one pixel, as in the HDF galaxy above. For WFC PSFs, for example, the blurring can cause a 10% reduction in the flux of the central pixel. This is not guaranteed, however; in one WFC PSF experiment with only four nearly exactly interlaced images, *Drizzle* produced a result that was apparently *sharper* than the Fourier reconstruction. Close examination, however, showed that the *Drizzle* result was still aliased; aliasing can cause features to be artificially sharpened as well as broadened. Further comparison of the Fourier method to *Drizzle* is thus best done in a context specific to the scientific problem at hand.

3.4. Noise in the Reconstructed Image

As alluded to in §3.1, the noise level in the reconstructed image depends on how well the dither pattern matches an ideal interlace pattern. For N images, the solutions presented in equations (24) or (25) reduce to a set of complex coefficients $\{c_n\}$ relating $F(u, v)$ to the data, as in the exact solution shown in equation (18). On the presumption that the noise from image to image is uncorrelated, then the average power in noise in the reconstructed image is simply

$$\eta_F = \left(\sum_{n=1}^{N} c_n^* c_n \eta_n^2 \right)^{1/2}, \tag{26}$$

where η_n is the noise power in image n. With a nearly ideal dither pattern (and equally-weighted data), $(c_n^* c_n)^{1/2} \approx K^2/N$, where K is the degree of subsampling; the noise level is as expected for the simple addition of N images. As the dither pattern becomes less ideal, however, unequal weight is placed on the images, depending on the uniqueness of their positions. Highly redundant images will have small coefficients, while more isolated images contribute relatively higher power. The linear combination of the images still produces an exact solution for the reconstructed image, but because the noise is incoherent from image to image it may be amplified in the final image, relative to its level in the ideal case. Equation (26) allows the noise in the reconstructed image to be calculated in advance for any particular dither pattern.

Figure 9 gives shows how the noise level in the reconstructed image varies as the dither pattern moves away from the ideal interlace for two examples of 2×2 subsampling. In these tests,

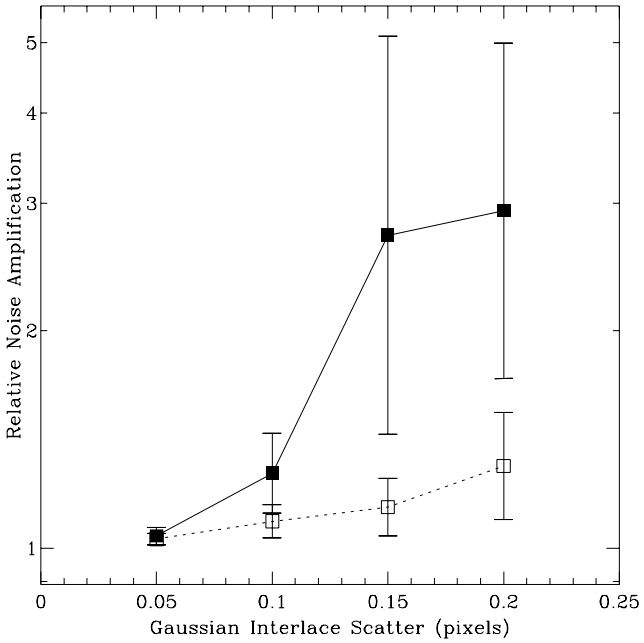

Fig. 9.— Simulations of the relative amplification of noise as a function of the departure of the dither pattern from a perfect interlace are shown. The departure is parameterized as a normal distribution of random offsets with the standard deviation specified in original pixels. The solid curve and points show the case for when only four images are used in the reconstruction. The dashed-line and open symbols show the simulations done with nine input images.

variations in the dither pattern were treated as random gaussian errors about the exact interlace. For a given standard deviation of the random offset, several simulated image reconstructions were computed. For the example with only four images, there is no redundant information, and the noise level depends strongly on the particulars of the dither pattern once excursions from the exact interlace become large. For nine images the reconstruction is more stable to departures from the ideal pattern, the final noise level showing less large excursions. The real importance of this demonstration, however, is to show that the noise level rises only slowly above its ideal for small errors in the dither pattern. Experience with WFPC-2, for example, shows that typical dithering errors ($\lesssim 0.1$ PC pixel) will give results within the regime of modest noise amplification.

4. Discussion and Summary

As noted in the introduction, my interest in the Fourier reconstruction method presented here stemmed from a strong desire to avoid the random blurring, Π', that *Drizzle* may introduce into the reconstructed image. The present method permits exact reconstruction of the superimage, with no blurring at the Nyquist scale, nor requires any arbitrary decisions or parameters to control the form of the reconstructed image. One might object that the degree of subsampling selected is such a parameter; however, it is really specified by the intrinsic spatial scale of the Nyquist frequency. A Nyquist-sampled image can be resampled at finer scales without loss of information content or introduction of artifact — images generated at various subsampling scales past the Nyquist scale are essentially equivalent representations of the image.

The present algorithm places several preconditions on the data, thus it is worthwhile to consider 1) the optimal data-taking strategy for reconstructing images from dithered data-sets, and 2) how to best perform the related tasks of artifact rejection, geometric rectification, and so on. The mathematics of the Fourier method strongly recommends selecting a dither pattern that contains fractional offsets as close to the ideal interlace pattern, itself. If a good dither pattern is realized, little is demanded of the linear combination of the images — one is simply accounting for the slight errors in its execution. It should be emphasized that the dither pattern can also contain integer pixel offsets as well, as might be desired to eliminate hot pixels, traps, blocked columns, and other fixed detector defects as well as cosmic rays. A nearly ideal program for the present algorithm would be to attempt a 2×2 subsampling interlace, but taking multiple exposures at each dither step to allow for cosmic ray rejection. This strategy clearly demands a rather large data-set, which may not be feasible for programs lasting only an orbit or two on *HST.* However, it presents no difficulties for multi-orbit programs, where one will be obtaining a large number of exposures in any case.

With regards to the second issue above, I have focused solely on the problem of reconstructing a Nyquist-sampled image. Tasks that are required before this stage include image registration and defect repair. Tasks that might follow reconstruction include geometric rectification, deconvolution, and filtering. *Drizzle* is attractive in part because it is a complete package that does many of

these steps together within the familiar IRAF/STSDAS environment. This said, however, I emphasize that many of the preliminary reduction steps can be done independently of the Fourier reconstruction algorithm — these issues should not impede its use. Indeed, one might use *Drizzle* for an initial reconstruction to provide for defect rejection prior to a second reconstruction cycle using the present algorithm. Geometric rectification is simple in principle if one is working with well-sampled images; the issue is generating such an image if geometric distortions are important in the undersampled observations. As noted earlier, if the dithers are small, scale changes across the image may be unimportant; if variations in the local dither step over the image domain are limited to a few percent of a pixel, then the entire domain may be reconstructed, and then later rectified. If the dither steps are large, however, the fractional pixel offsets may vary significantly over the image, requiring the reconstruction to be done in subsets of the domain and later patched together. This may be unattractive for some problems requiring panoramic imaging, but may be irrelevant if the primary objects of interest are compact or occupy only small portions of the images.

While the Fourier reconstruction method presented here works only for translational dithers, in passing, I note that the professional image processing literature does contain algorithms related to be present one that can combine undersampled images with more complex geometric interrelationships. Granrath & Lersch (1998) present an algorithm that constructs a Nyquist-sampled image from an image set whose members can be related to each other with affine transformations, i. e., the geometric transformations that include rotation, scale change, and shear, as well as simple translations. The Granrath & Lersch algorithm constructs a "projection-onto-convex-sets" estimate that gives the best reproduction of the image set, in contrast to the present method, which yields a closed-form solution to the Nyquist image. Methods of this sort may be of interest in cases where the image does not meet the conditions required for the present Fourier method, but precise treatment of the Nyquist-scale is still important.

In summary, the Fourier technique presented here may not be the first choice to construct a Nyquist image when the geometrical relationships among the image set are complex, or the dither pattern is strongly non-optimal. Further, its resolution gains may appear to be superficially modest. Regardless, there remains a class of *HST* imaging problems that push right against the diffraction scale of the instrument. This class includes crowded field stellar photometry, the nuclear structure of galaxies — particularly those with bright AGN, the morphology of lensed QSOs, and so on. This method allows clean access to the Nyquist scale and should be of use for these problems and more.

I wish to thank Bobby Hunt, Christoph Keller, and Ken Mighell for useful conversations.

REFERENCES

Bracewell, R. N. (1978), The Fourier Transform and its Applications, p. 201-202 (McGraw-Hill)

Cohen, J. G., Cowie, L. L., Hogg, D. W., Songaila, A., Blanford, R., Hu, E. M., & Shopbell, P. (1996), ApJ, 471, L5

Fruchter, A. S. & Hook, R. N. (1998) PASP, submitted; astro-ph/9808087

Granrath, D. & Lersch, J. (1998), J. Opt. Soc. Am. A, 15, 791

Kim, S. P., Bose, N. K., & Valenzuela, H. M. (1990), IEEE Transactions on Acoustics, Speech, and Signal Processing, 38, 1013

Lauer, T. R., Ajhar, E. A., Byun, Y.-I., Dressler, A., Faber, S. M., Grillmair, C., Kormendy, J., Richstone, D., & Tremaine, S. 1995, AJ, 110, 2622

Tsai, R. Y. & Huang, T. S. (1984) in *Advances in Computer Vision and Image Processing,* 1, 317 (JAI:Greenwich)

Williams, R. E. et al. (1996), AJ, 112, 1335

This preprint was prepared with the AAS LaTeX macros v4.0.